

JD2449112 we exposed Θ^1 Ori C in 89 nights. The typical exposure time was one hour. As evidenced by Figure 6, the spectrum of Θ^1 Ori C is distinguished by extremely regular variations of $H\alpha$, the period being 15.43 ± 0.03 days (see Stahl et al. 1993b). In the Figure, the nebular emission (white) is shifted so that a range of -600 to $+300$ km s $^{-1}$ around $H\alpha$ is displayed. Continuum is blue. Blue-shifted stellar emission and absorption alternate very regularly with virtually no difference from cycle to cycle. The apparent deviation during the fifth period is caused by worse sampling due to bad weather. Note that the discernible substructure in the black stripes is due to a second maximum of (redshifted) emission. This same strict periodicity was also found for HeII 4686 and other different lines. Θ^1 Ori C is a good example to show the importance of having long time series with regular sampling and good resolution in time. Based on previous snap shot observa-

tions, the inverse P Cygni-type emission of HeII 4686 "occurred on an irregular fashion" and was therefore ascribed to accretion rather than to something strictly connected to the rotation of Θ^1 Ori C. The strict periodicity now established does, however, favour such a connection and makes Θ^1 Ori C the first convincing candidate of an O star oblique rotator.

Conclusion

The results presented demonstrate the considerable impact of long-term high-resolution spectroscopic monitoring programmes at small telescopes on variable star research.

The ESO 50-cm telescope, our fiber-linked echelle spectrograph and the excellent meteorological conditions of the Atacama desert – a perfect match for investigating the long-term spectroscopic behaviour of bright stars.

References

- Conti, P.: 1972, *ApJ*, **170**, 325.
Mandel, H.: 1988, in IAU Symp. 132, eds. G. Cayrel de Strobel and M. Spite, p. 9–13, Kluwer.
Stahl, O., Mandel, H., Wolf, B., Gäng, Th., Kaufer, A., Kneer, R., Szeifert, Th. Zhao, F.: 1993a, *A&AS*, **99**, p. 167–177.
Stahl, O.: 1993, in *New Aspects of Magellanic Cloud Research*, eds. B. Baschek, G. Klare, J. Lequeux (Proc. Sec. European Meeting on the Magellanic Clouds, SFB 328), p. 263.
Stahl, O., Wolf, B., Gäng, Th., Gummertsbach, C.A., Kaufer, A., Kovacs, J., Mandel, H., Szeifert, Th.: 1993b, *A&A*, **274**, L29–L32.
Sterken, C.: 1977, *A&A*, **57**, 361.
Sterken, C., Gosset, E., Jüttner, A., Stahl, O., Wolf, B., Axer, M.: 1991, *A&A*, **247**, 383.
van Genderen, A.M.: *A&A*, **208**, 135.
Wolf, B.: 1989, *A&A*, **217**, 87.
Wolf, B.: 1992, in *Nonisotropic and Variable Outflows from Stars*, eds. L. Drissen, C. Leitherer, A. Nota, (A.S.P. Conf. series Vol. 22), p. 327.

Probing the Kinematics in the Core of the Globular Cluster M15 with EMMI at the NTT

P. DUBATH and G. MEYLAN, ESO

D. QUELOZ and M. MAYOR, Geneva Observatory, Switzerland

1. M15: a Prototype Collapsed-Core Cluster?

There is now a global theoretical understanding of the long-term dynamical evolution of globular clusters. Different kinds of theoretical approaches predict the collapse of the cluster core, which can then be halted or even reversed by a core heating due to stellar encounters involving binary stars. A cluster could suffer a succession of collapsing and expanding phases: the so-called gravothermal oscillations (for recent reviews see the proceedings of the workshop *Structure and dynamics of globular clusters*, Djorgovski and Meylan eds. 1993).

From an observational point of view, however, the situation is much less clear (see e.g. Meylan 1993). A major difficulty in finding a signature of core collapse in a globular cluster is that the observable structural changes may occur only in a very small central area, where accurate measurements of surface brightnesses and velocity dispersions are greatly complicated by the small number of bright stars dominating the integrated light. In the case of the high-concentration globular cluster M15,

considered for a long time as a prototype of the collapsed-core star clusters, the observational difficulties are particularly important.

The current determinations of the surface-brightness profile of M15 do not allow us to discriminate between pre- and post-core collapse models, nor to exclude the presence of a central massive black hole. Although the central luminosity cusp in M15 has now been clearly resolved into several bright stars (see Figures 1 and 2), even the most recent studies from HST data cannot unambiguously determine whether the surface-brightness radial profile flattens off interior to a radius of about 2" or continues to rise at subarcsecond radii (see Lauer et al. 1991 and Yanny et al. 1993). The central velocity dispersion profile in M15 is also poorly known. Accurate central velocity dispersions are difficult to obtain from radial velocities of individual stars because of crowding and the small number of bright stars. An alternative is to use integrated-light spectra to derive velocity dispersions by measuring the line broadening that arises from the random motions of the stars. In this way, Peterson et al.

(1989) obtained velocity dispersion values $8.4 \leq \sigma_p \leq 30.0$ km s $^{-1}$ over different small ($\sim 1''$) areas of integration in the central few arcseconds of M15. They retain as their best estimate a central velocity dispersion of 25 km s $^{-1}$, a value difficult to reconcile with any existing model, and possibly indicative of the presence of a central black hole. More recently, we derived a velocity dispersion of 14 km s $^{-1}$ from an integrated light spectrum obtained over a central area of integration of $6'' \times 6''$ (Meylan et al. 1991, Dubath et al. 1993, 1994). Because of our larger sampling area, we probably would have missed any central velocity dispersion cusp over an area of $\sim 1''$. However, recent numerical simulations (Zaggia et al. 1992a, b, and Dubath et al. 1993, 1994) pointed out that the velocity dispersions derived over such small central areas in M15 are affected by large statistical errors because of the dominance of too small a number of bright stars. These errors can explain the large variation of velocity-dispersion estimates obtained at different locations in the core of M15.

In order to test the existence of a central velocity dispersion cusp in the

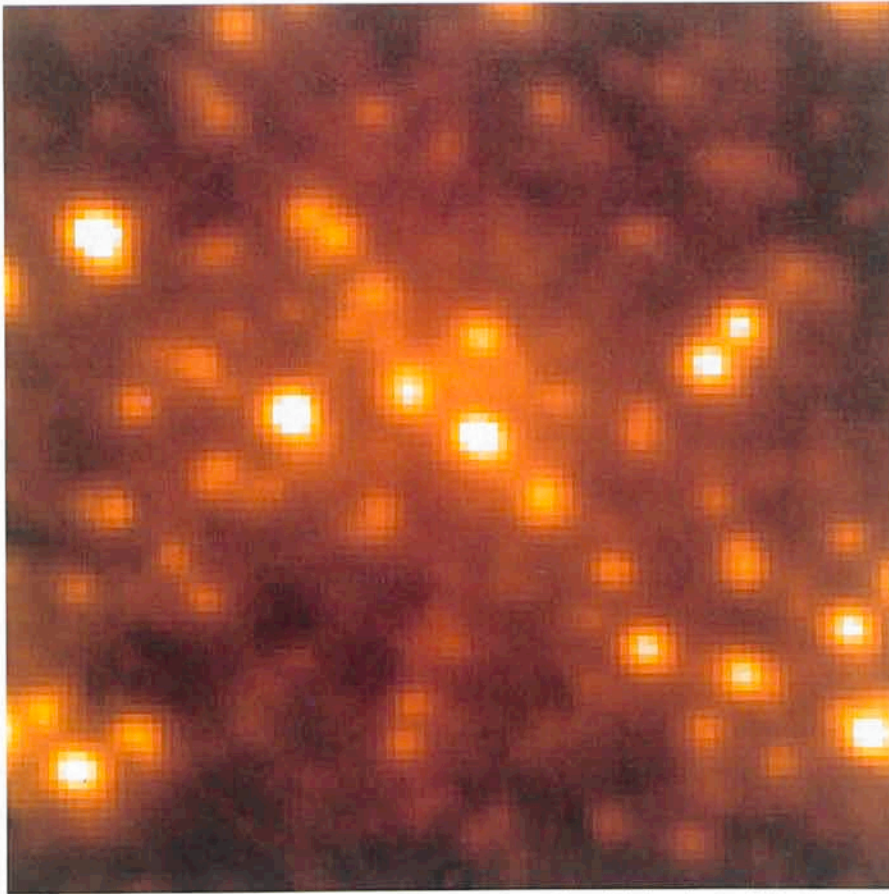
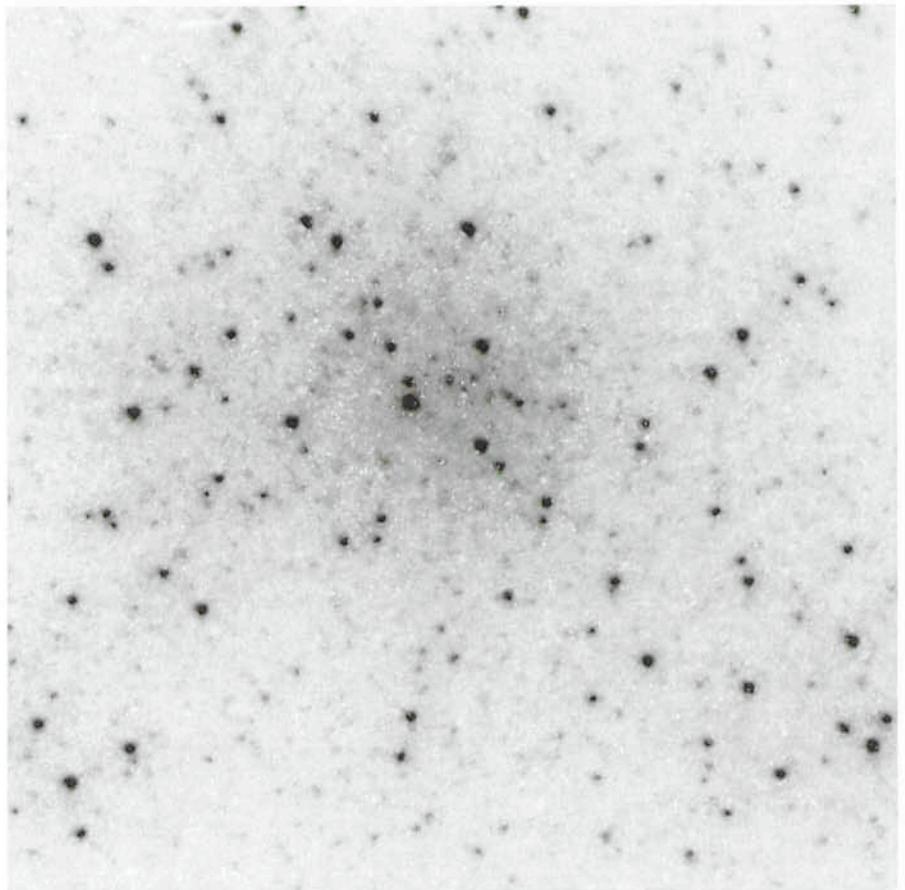


Figure 1: CCD image of the central 10.5" square region of the globular cluster M15 taken in the V-band with HRCam at the CFHT (from Racine & McClure 1989). The angular resolution on this image is 0.35" FWHM. The three stars, forming an equilateral triangle at the centre of the figure, are the main contributors to the former unresolved luminosity cusp.

core of M15, we carried out new high-resolution observations with the ESO Multi-Mode Instrument (EMMI) on the NTT. The best way to minimize the statistical error due to a small stellar sample is to obtain a full 2-D kinematical map of the cluster core, i.e., to derive radial velocities and velocity dispersions at many different locations. The unique imaging/spectroscopic capabilities of EMMI are very useful to carry out such observations. CCD images taken just before an echelle spectrum allow very precise *a priori/posteriori* positioning of the slit within the crowded core of M15.

Figure 2: The same region of M15 as in Figure 1, as seen by the Faint Object Camera (FOC) of the HST (Dubath et al. 1994). This public image was obtained in the F/96 mode with the F342 (central wavelength 3420 Å) filter. The sharp cores of the point spread functions have FWHM = 0.08". No image restoration has been applied to this image. The three central stars are even more prominent at this wavelength than in the V-band image (Figure 1).



2. Mapping the Core of M15 with EMMI Observations

In July 1993, we obtained five high-resolution integrated-light echelle spectra in the core of M15. We used a 1"×8" slit, with exposures offset in 1" steps in order to cover a total central area of 5"×8" (see Figure 3). The exposure times were ~30 minutes for each exposure. During these observations, the seeing values (determined from EMMI CCD images) were about 0.9". EMMI was used in echelle mode with the echelle grating #10 and the cross-dispersing grism #5 (see the EMMI operating manual). The CCD used is the ESO CCD #34. It is a LORAL CCD with 2048×2048 pixels of a size of 15 μm which correspond to 0.35" on the sky. For our instrument setup and slit width, the typical full-width at half-maximum (FWHM) of the emission lines of the thorium-argon comparison spectra, i.e., our typical spectral resolution, is 9–10 km s⁻¹.

Before each exposure on the cluster core, we also obtained (1) an echelle spectrum of an isolated red giant member of M15, and (2) CCD images of the core of M15 in the V-band. The observations of red giant stars show that the width of stellar cross-correlation functions is perfectly constant during all the observations and small (6.5 km s⁻¹).

in comparison with the expected central velocity dispersion ($10\text{--}25\text{ km s}^{-1}$) in M15. The width of the cross-correlation functions of stars depends mostly, when the intrinsic width of the stellar lines is small, on the spectral resolution of the observations.

The CCD images were first used to position the slit with the usual procedure. A bright isolated star is accurately centred on the slit in echelle mode using the slit viewer. EMMI is switched to the imaging mode, and the position on the CCD corresponding to the slit position in echelle mode is determined from an image of the star. The telescope is then shifted to move the cluster location to be observed to the same pixel coordinates as those of the bright star, and EMMI is switched back to the echelle mode to start the spectral observation. These CCD images also allow a *posteriori* check of the slit position. The intensity profile through the slit is compared with that from the CCD image at the expected slit location. Thanks to the crowded stellar field in the core of M15, a good match between the two profiles is only obtained at one location on the CCD. Moving by one pixel in any direction degrades significantly the agreement between the two intensity profiles. In this way, we can determine the position of the slit to better than half a pixel, i.e., to better than $0.2''$. The exact locations of the $1''\times 8''$ slit during the five high-resolution spectral observations are displayed in Figure 3.

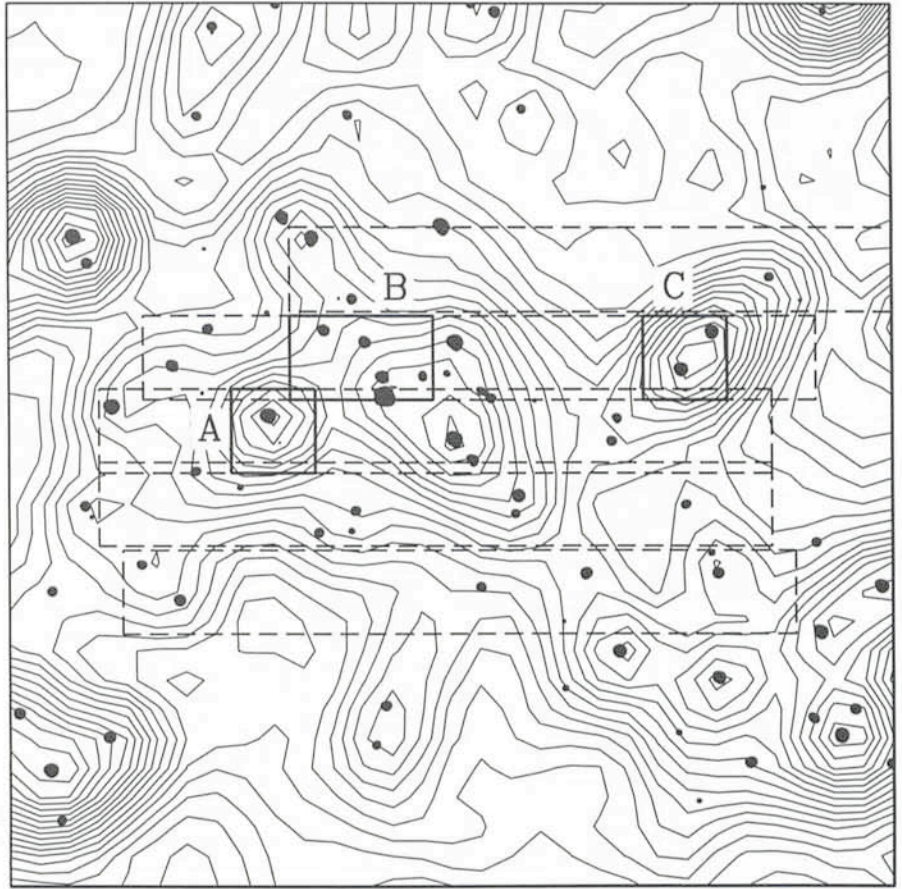


Figure 3: In this figure, the HST image from Figure 2, displayed with a high low-cut-off so as to show only the bright stars of this image as black dots, is superposed to isomagnitude contours from one of the V-band CCD images taken with EMMI at the NTT. The isolated stars of the EMMI image have FWHM of $0.9''$. The five dashed-line rectangles show the exact positions of the $1''\times 8''$ slit during the five high-resolution spectral observations on the cluster core. The three solid-line rectangles are three particular areas of integration for which the corresponding cross-correlation functions are displayed in Figure 4.

3. Data Reduction with INTER-TACOS

The data reduction was carried out with a new software called INTER-TACOS (INTERpreteur-Treatment, Analysis, CORrelation of Spectra) developed by L. Weber and D. Queloz at the Geneva Observatory. This programme is built and optimized for the automatic data reduction of echelle spectra from fiber-fed spectrographs but is also efficient for images from slit spectrographs. INTER-TACOS is now in operation at the Observatoire de Haute-Provence to do on-line the automatic data reduction of spectra from the ELODIE echelle spectrograph.

This software includes a cross-correlation package which works easily with very low signal-to-noise images, typically used for cross-correlation analysis. Optimal orders extraction and very efficient cosmic correction algorithms (Horne 1986) are available. Great care was taken to define a good wavelength calibration algorithm. Using about 1000 calibration lines, we measured with ELODIE at the OHP a wavelength calibration reproducibility of 2 m/s . The

cross-correlation algorithms work with 2-D spectra (orders – pixels) and a wavelength solution stored in coefficients. The different orders are neither rebinned in wavelength units, nor merged together.

The five echelle spectra of the cluster core were reduced by taking advantage of the spatial resolution along the slit, as for long slit spectra. The spatial information along the slit of EMMI in echelle mode is fully conserved. We checked this by observing isolated stars positioned at different locations along the slit. In addition, with a slit of $8''$ in length and the EMMI setup used, the successive orders do not overlap.

For each of the five observations in the cluster core (see Figure 3), we extracted spectra from each order in many spatial bins along the slit direction. These spectra were then reduced using INTER-TACOS, and the reduced spectra cross-correlated with a numerical mask. The properties of this mask, as well as the details of our cross-correlation technique, are described in previ-

ous studies (e.g., Dubath, Meylan and Mayor 1992). Our cross-correlation technique produces a cross-correlation function (CCF) – relative intensity as a function of the radial velocity V_r – which is nearly a perfect Gaussian (see Figure 4). The radial velocity is given by the abscissa of the minimum of the CCF, and the velocity dispersion can be derived from the broadening of the CCF in comparison with CCFs of individual stars.

4. Results

The radial velocity and the broadening of the cross-correlation function were derived for each pixel position in the area covered by the five slits displayed in Figure 3. The spatial resolution of these measurements is limited in one direction by the slit width ($1''$) and in the other direction – along the slit – by the seeing ($\sim 0.9''$). This kinematical map fully confirms the results of our numerical simulations (Dubath et al. 1994) which predicted large statistical errors,

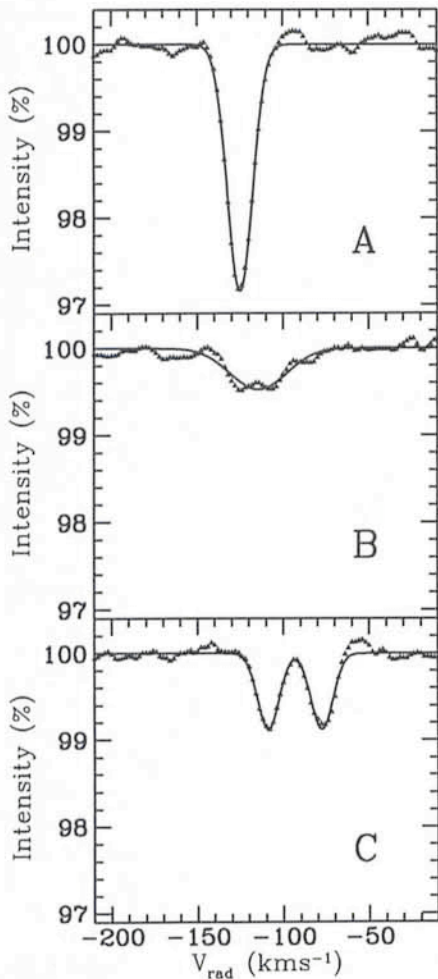


Figure 4: Cross-correlation functions of the integrated light spectra taken over three particular areas of integration illustrated by the three solid-line rectangles in Figure 3. The CCF A has a stellar width and allows us to derive an accurate radial velocity for the star located in the rectangle A in Figure 3. The double CCF C shows that the two stars in rectangle C, barely spatially resolved, are clearly resolved in velocity by our observations. In the case B, we have integrated over a slightly larger area in order to produce a CCF as large as possible. The velocity dispersion derived from the broadening of the CCF B is 15 km s^{-1} .

due to small samples, on the velocity dispersion measurements derived from integrated light spectra taken over small areas of integration at the centre of M15. The CCFs derived at the locations of the brightest stars are not significantly larger than the CCF of isolated stars. Around these locations, the CCFs are barely broadened, and any velocity dispersion measurement derived from these CCFs would underestimate strongly the real velocity dispersion. At other locations, the CCFs are clearly double (or triple) and sometimes two (or three) spatially unresolved stars appear to be spectroscopically resolved. In

these cases, if the few dominant stars have unusually large radial velocity differences, the CCFs are artificially broadened leading to overestimates of the velocity dispersion. These different cases are illustrated in Figure 4, which shows three CCFs A, B, and C obtained respectively from the area of integration A, B, and C displayed in Figure 3. The CCF A has a stellar width and allows us to derive an accurate radial velocity for the star (AC 212, Aurière and Cordoni 1981) located in the rectangle A in Figure 3. The double CCF C shows that the two stars (AC # 214 and # 215) in rectangle C, barely resolved under the seeing conditions during the observations, are clearly resolved in velocity. Accurate radial velocities were also derived for these two stars. In the case B, we have integrated over a slightly larger area in order to produce a CCF as large as possible. The velocity dispersion derived from the broadening of the CCF B is 15 km s^{-1} , however, the statistical error on this result is large since the CCF B includes mostly the contributions of three stars. This is not obvious from Figure 4B, but appears unambiguously in CCFs obtained over smaller spatial bins.

The broadening of the cross-correlation functions is always $\leq 17 \text{ km s}^{-1}$, at any location in the $5'' \times 8''$ central area mapped. Our numerical simulations show that this value provides very probably an upper limit for the central velocity dispersion. The CCFs of integrated spectra taken at locations away from the brightest stars are less affected by statistical errors due to small samples and give velocity dispersions $10 \leq \sigma_p \leq 15 \text{ km s}^{-1}$. In order to minimize the statistical error due to a small sample, one can reduce the domination of the few brightest stars by taking the average of the *normalized* CCFs over all locations in the $5'' \times 8''$ central area. In this way, a velocity dispersion of 11.7 km s^{-1} is derived.

The radial velocities of the 14 best resolved (spatially or spectroscopically) bright stars were also determined. The velocity dispersion from these stars is $16.0 \pm 3.0 \text{ km s}^{-1}$. This value is also likely to be an upper limit, since stars with large relative velocities are more easily spectroscopically resolved. We have radial velocities for two of the three brightest stars (AC # 214, 215, 216, the three bright stars in the centre of Figure 1 and 2) of the former unresolved cusp, the third being too blue to provide a radial velocity. Two of the brightest stars, separated by $2.5''$, AC # 212 and 215, have radial velocity values differing by 48.9 km s^{-1} . A brief account of these results is published in Meylan and Dubath (1993).

5. Conclusion

We do not find any evidence for a velocity cusp in M15 from our mapping of the kinematics in the central area of $5'' \times 8''$. There is no evidence for a central velocity dispersion significantly larger than 15 km s^{-1} , and our best estimate is $\sigma_p = 13 \pm 3 \text{ km s}^{-1}$. This value is consistent with predictions of several pre- or post-collapse theoretical dynamical models of M15: $\sigma_p(0) = 12\text{--}17 \text{ km s}^{-1}$ from Illingworth and King (1977), $\sigma_p(0) = 13\text{--}15 \text{ km s}^{-1}$ from Phinney and Sigurdsson (1991) and Phinney (1993), and $\sigma_p(0) = 14 \text{ km s}^{-1}$ from Grabhorn et al. (1992). Consequently, there is no need to invoke the presence of any massive central black hole in the core of M15.

References

- Aurière, M., & Cordoni, J.-P. 1981, *A&A*, **100**, 307.
- Dubath, P., Meylan, G., & Mayor, M. 1992, *ApJ*, **400**, 510.
- Dubath, P., Mayor, M., & Meylan, G. 1993, in *Structure and Dynamics of Globular Clusters*, ASP Conference Series, Vol. 50, eds. S. Djorgovski & G. Meylan (San Francisco: ASP), p. 69.
- Dubath, P., Meylan, G., & Mayor, M. 1994, *ApJ*, in press.
- Grabhorn, R.P., Cohn, H.N., Lugger, P.M., & Murphy, B.W. 1992, *ApJ*, **392**, 86.
- Horne, K. 1986, *PASP*, **98**, 609.
- Illingworth, G., & King, I.R. 1977, *ApJ*, **218**, L109.
- Lauer, T.R., Holtzman, J.A., Faber, S.M., Baum, W.A., Currie, D.G., Ewald, S.P., Groth, E.J., Hester, J.J., Kelsall, T., Light, M., Lynds, C.R., O'Neil, E.J., Schneider, D.P., Shaya, E.J., & Westphal, J.A. 1991, *ApJ*, **369**, L45.
- Meylan, G. 1993, in *Ergodic Concepts in Stellar Dynamics*, eds. D. Pfenniger and V.G. Gurzadyan (Berlin: Springer), in press.
- Meylan, G., Dubath, P., & Mayor, M. 1991, *BAAS*, **23**, 833.
- Meylan, G., & Dubath, P. 1993, *BAAS*, **23**, in press.
- Phinney, E.S., & Sigurdsson, S. 1991, *Nat.*, **349**, 220.
- Phinney, E.S. 1993, *MNRAS*, in press.
- Peterson, R.C., Seitzer, P., & Cudworth, K.M. 1989, *ApJ*, **347**, 251.
- Racine, R. & McClure, R.D. 1989, *PASP*, **101**, 731.
- Yanny, B., Guhathakurta, P., Schneider, D.P., & Bahcall, J.N. 1993, *ApJL*, in press.
- Zaggia, S., Capaccioli, M., & Piotto, G. 1992a, in *Star Clusters and Stellar Evolution*, eds. E. Brocato, F. Ferraro, & Piotto, *Mem. Soc. Astron. Ital.*, **63**, 211.
- Zaggia, S., Capaccioli, M., Piotto, G. & Stiavelli, M. 1992b, *A&A*, **258**, 302.